

Explainability-Aware Evaluation of Transfer Learning Models for IoT DDoS Detection Under Resource Constraints

Nelly Elsayed^{a,1}

¹School of Information Technology, University of Cincinnati, Ohio, United States

Received: date / Accepted: date

Abstract Distributed denial-of-service (DDoS) attacks threaten the availability of Internet of Things (IoT) infrastructures, particularly under resource-constrained deployment conditions. Although transfer learning models have shown promising detection accuracy, their reliability, computational feasibility, and interpretability in operational environments remain insufficiently explored. This study presents an explainability-aware empirical evaluation of seven pre-trained convolutional neural network architectures for multi-class IoT DDoS detection using the CICDDoS2019 dataset and an image-based traffic representation. The analysis integrates performance metrics, reliability-oriented statistics (MCC, Youden Index, confidence intervals), latency and training cost assessment, and interpretability evaluation using Grad-CAM and SHAP. Results indicate that DenseNet and MobileNet-based architectures achieve strong detection performance while demonstrating superior reliability and compact, class-consistent attribution patterns. DenseNet169 offers the strongest reliability and interpretability alignment, whereas MobileNetV3 provides an effective latency-accuracy trade-off for fog-level deployment. The findings emphasize the importance of combining performance, reliability, and explainability criteria when selecting deep learning models for IoT DDoS detection.

Keywords Internet of Things · DDoS Detection · Transfer Learning · Explainable AI · Model Reliability

1 Introduction

The Internet of Things (IoT) has emerged as a foundational component of modern digital infrastructures [1, 2].

^ae-mail: elsayeny@ucmail.cu.edu

It has been widely deployed across large-scale domains, including industrial systems [3, 4, 5], healthcare infrastructures [6, 7, 8], and enterprise networks [9], as well as in smaller-scale environments such as smart homes [10, 11, 12], small businesses [13, 14], and office settings [15]. While IoT enables automation and real-time monitoring, its rapid expansion significantly amplifies exposure to various cyber threats [16, 17]. The integration of resource-constrained devices, heterogeneous communication protocols, and distributed architectures introduces substantial security vulnerabilities that can affect hardware assets, sensitive data, and, most critically, system availability [18]. Therefore, securing IoT infrastructure and ensuring resilience are primary cybersecurity concerns.

Denial of Service (DoS) and Distributed Denial of Service (DDoS) attacks are the most severe threats to IoT-driven environments [19, 20]. These attacks aim to exhaust bandwidth, computational capacity, or protocol state resources by generating overwhelming traffic volumes [21, 22]. The resulting resource depletion leads to partial or complete service disruption for legitimate users [23, 24]. From a cybersecurity perspective, such attacks directly violate the availability principle of the pillars of information security: Confidentiality-Integrity-Availability (CIA) triad [25], which is shown in Figure 1, which represents the foundational framework for information security [26]. Therefore, preserving availability in IoT infrastructures is essential to maintaining operational continuity and preventing large-scale service outages.

Recent reports indicate a substantial increase in DDoS activity worldwide. According to VERCARA, the industry analysis report shows a significant year-over-year growth in volumetric and reflection-based DDoS campaigns targeting telecommunications, finance, and

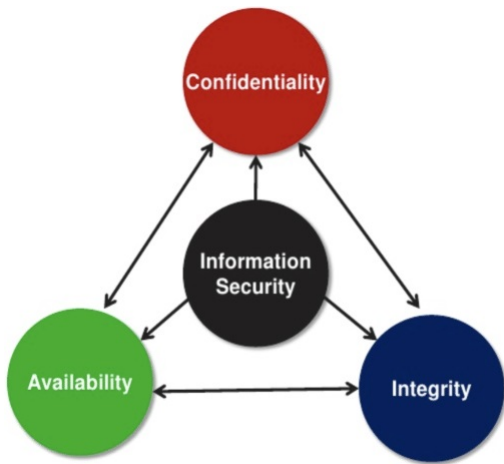


Fig. 1: The cybersecurity CIA triad that represents the three pillars of information security: confidentiality, integrity, and availability [25].

service providers [27]. IoT environments are particularly vulnerable due to limited computational resources, constrained memory, and often insufficient built-in security mechanisms [28, 29].

DDoS attacks against IoT networks can take multiple forms, such as volumetric flooding attacks, protocol exploitation attacks, and application-layer attacks [28, 30, 31]. Reflection and amplification techniques, leveraging services such as DNS, NTP, SSDP, and LDAP, enable attackers to magnify traffic volume while spoofing source addresses. Such attacks are commonly executed via botnets comprising compromised devices geographically distributed across multiple regions. [32, 33, 34]. The distributed nature of botnets makes detection and mitigation particularly challenging [35, 36, 37].

Traditional detection mechanisms, such as firewalls, rule-based intrusion detection systems (IDS), and manual traffic monitoring, often struggle to sustain performance under complex and multi-vector DDoS attacks [38, 39, 40]. Thus, machine learning and deep learning approaches have increasingly been adopted to identify anomalous traffic patterns [41, 42, 43, 44, 45, 46, 47, 48, 49, 50, 51]. However, several practical challenges remain insufficiently addressed. Many existing studies prioritize detection accuracy while overlooking computational cost, inference latency, deployment feasibility in resource-constrained IoT environments, and the reliability and transparency of model decisions [52, 53].

In this paper, we aim to address these challenges through a security-grounded empirical evaluation of pre-trained deep learning models for DDoS detection in IoT infrastructures. Specifically, this paper investigates the following core questions: (i) How effectively can pre-trained models detect heterogeneous DDoS attack

types in IoT environments? (ii) What are the computational and latency trade-offs associated with deploying such models under fog-level resource constraints? (iii) To what extent can explainable artificial intelligence techniques enhance the reliability and transparency of detection decisions?

To answer these questions, we evaluate multiple lightweight and advanced pre-trained models using a benchmark IoT DDoS dataset. The study analyzes detection performance, computational overhead, and inference time, and integrates SHAP and Grad-CAM explainability methods to assess decision reliability [54, 55]. This paper aims to support the development of reliable and transparent DDoS detection mechanisms for resource-constrained IoT infrastructures by combining performance evaluation with interpretability analysis.

2 Threat Model and Security Assumptions

This paper considers a distributed denial-of-service (DDoS) threat targeting IoT-driven network infrastructures. The threat model is defined to formally characterize adversarial capabilities, defender assumptions, and the security objectives guiding the proposed detection framework [56, 57].

2.1 Adversary Model

We assume a remote adversary controlling a botnet composed of compromised devices capable of generating high-volume traffic toward a target IoT infrastructure. The attacker can launch volumetric, protocol-based, and application-layer DDoS attacks, including reflection and amplification attacks such as DNS, NTP, SSDP, LDAP, MSSQL, UDP floods, SYN floods, and related variants [58, 59, 60, 61, 62, 63]. The adversary is capable of generating large-scale distributed traffic from multiple sources, spoofing source IP addresses in reflection-based attacks, and varying attack strategies across known DDoS categories to exhaust network and computational resources.

However, the adversary is not assumed to perform adversarial machine learning attacks such as model poisoning during training or evasion through carefully crafted perturbations targeting model decision boundaries [64, 65]. Furthermore, we assume that the attacker does not gain direct access to modify or tamper with the deployed detection model. The focus of this paper is on network-level DDoS detection rather than adversarial ML robustness.

2.2 Defender Model

The defender operates at the fog or gateway level within the IoT infrastructure, where traffic is monitored and detected before reaching core services [66, 67, 68]. The detection system monitors network flow-level features extracted from traffic without performing deep packet inspection or payload analysis [69]. The model is trained offline using labeled data and deployed for real-time inference to support timely attack identification [70, 71].

The defender’s objectives are to achieve reliable detection of DDoS attacks while preserving service availability. In particular, minimizing false negatives is critical to prevent prolonged service disruption. Whereas controlling false positives is essential to reduce unnecessary mitigation actions and operational overhead [72, 73].

2.3 Security Objectives

The primary security goal of the proposed framework is to preserve the availability of IoT-driven systems under DDoS conditions. To achieve this objective, the detection mechanism aims to provide timely and accurate identification of attack traffic, maintain stability across heterogeneous attack categories, and support security assurance through explainable decision-making. By integrating performance evaluation with interpretability analysis, the framework seeks to enhance transparency and trust in automated detection within resource-constrained IoT environments.

3 Background and Related Work

3.1 IoT Architecture and Attack Surface

IoT infrastructures are commonly organized into three logical layers: the perception layer, the network layer, and the application layer, as illustrated in Figure 2. The perception layer comprises sensors and embedded devices that acquire data. The network layer enables communication between IoT devices, gateways, and external services through heterogeneous wired and wireless protocols. The application layer delivers monitoring, analytics, and control services [74, 75].

The distributed and heterogeneous nature of IoT systems increases the attack surface, particularly at the network layer, where traffic aggregation and routing occur. Limited computational capacity, constrained memory, and inconsistent security configurations further amplify vulnerability to availability-oriented attacks [77]. As IoT deployments scale across industrial and enterprise en-

vironments, protecting network availability becomes a central security requirement.

3.2 DDoS Threats in IoT Environments

Distributed denial-of-service (DDoS) attacks remain among the most prevalent threats to IoT infrastructures [28, 78, 79]. Such attacks aim to exhaust bandwidth, computational resources, or protocol state tables by generating high volumes of malicious traffic [80, 81]. In IoT environments, attackers frequently exploit reflection and amplification mechanisms (e.g., DNS, NTP, SSDP, LDAP) to magnify traffic volume while spoofing source addresses [82].

Botnets composed of compromised IoT devices enable geographically distributed traffic generation at scale [83, 33, 34]. Due to limited built-in security mechanisms and irregular patch management, IoT devices often serve both as attack targets and as components of attack infrastructure. Consequently, reliable and efficient DDoS detection mechanisms are essential to preserve service availability in IoT-driven systems.

3.3 Machine Learning-Based DDoS Detection

Traditional rule-based intrusion detection systems and signature-based mechanisms often struggle to cope with large-scale, multi-vector DDoS campaigns [43, 38]. To address these limitations, machine learning (ML) and deep learning (DL) techniques have been widely adopted for traffic classification and anomaly detection in IoT environments.

Prior studies have explored classical ML algorithms, including support vector machines, random forests, extreme learning machines, and k-nearest neighbors, for DDoS detection using handcrafted traffic features. More recently, deep neural networks, convolutional neural networks (CNNs), and recurrent architectures have demonstrated improved detection accuracy by learning complex traffic patterns directly from data [43, 84, 44, 85, 45]. Transfer learning approaches using pre-trained CNN architectures have also been investigated to reduce training cost and leverage feature extraction capabilities developed in large-scale image classification tasks [46, 86].

Despite promising detection performance, several limitations persist in the existing literature. Many studies emphasize classification accuracy while providing limited analysis of computational cost, inference latency, and deployment feasibility in resource-constrained IoT or fog-level environments [86, 87, 88]. In addition, reliability evaluation is often restricted to aggregate performance metrics without examining stability across

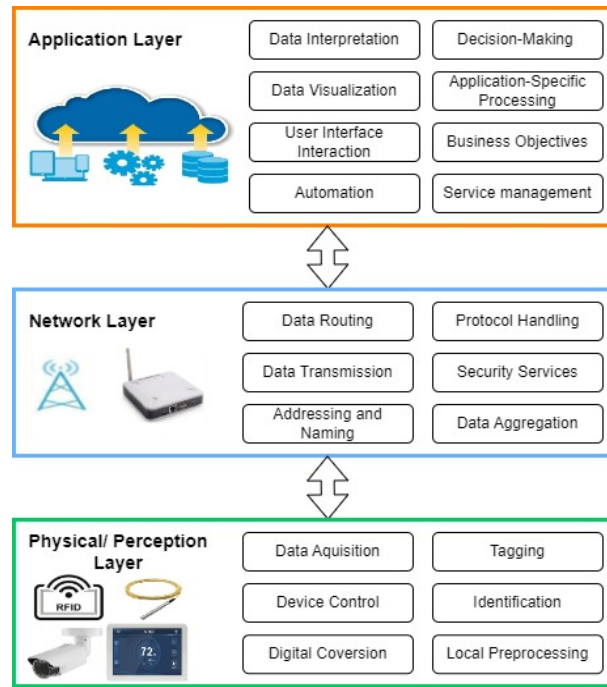


Fig. 2: The IoT three-layered architecture [76].

heterogeneous attack types [38]. Moreover, explainability and interpretability of deep learning-based detection models remain underexplored, raising concerns regarding transparency, trustworthiness, and forensic usability in operational settings.

In this paper, we address these gaps by providing a comprehensive security-oriented evaluation of pre-trained deep learning models for IoT DDoS detection. The proposed framework integrates performance assessment, computational cost analysis, and explainability evaluation to support reliable and transparent deployment under practical resource constraints.

4 Research Methodology

In this section, we present the research components and methodology of this empirical and analytical study to answer the core research questions. The objective is to systematically evaluate pre-trained deep learning models for detecting DDoS attacks in IoT-driven environments under realistic deployment constraints.

To ensure transparency, reproducibility, and fair comparisons among models, we employed a publicly available benchmark dataset designed for DDoS attacks. Using a standardized dataset allows the research community to replicate and extend the proposed study in future investigations.

The overall research methodology adopted for investigating the pre-trained models for DDoS attack detection is shown in Figure 3.

4.1 Dataset

In this study, we used the CICDDoS2019 benchmark dataset [38], which is publicly available and widely adopted in DDoS detection research. The dataset contains labeled network traffic flows representing benign traffic and multiple DDoS attack categories [89, 84]. The considered attack types include DNS amplification, LDAP amplification, MSSQL reflection, NetBIOS, NTP amplification, SNMP amplification, SSDP, UDP flood, SYN flood, TFTP amplification, and UDP-Lag attacks.

Each attack category reflects distinct traffic characteristics, including volumetric flooding, protocol exploitation, and reflection-based amplification mechanisms. This diversity enables evaluating model robustness across heterogeneous attack patterns.

The dataset was preprocessed by removing duplicate records, incomplete samples, and constant-valued features to reduce redundancy and eliminate non-informative attributes. Feature scaling was performed using min-max normalization to ensure consistent value ranges across all features. The normalization process is defined as:

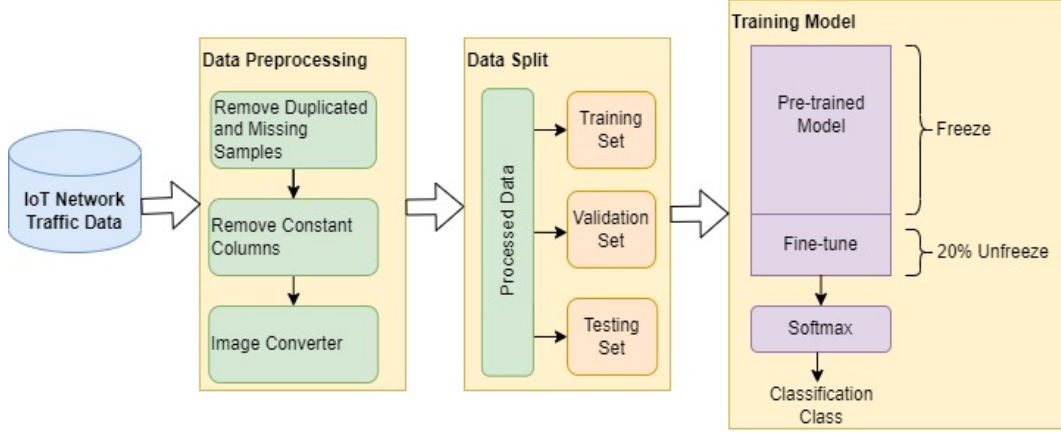


Fig. 3: The proposed research methodology for investigating pre-trained models for DDoS attack detection.

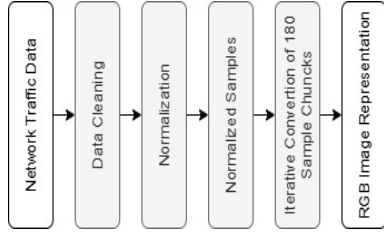


Fig. 4: Network traffic data transformation into image representation for pre-trained models.

$$X' = \frac{X - \min(X)}{\max(X) - \min(X)} \times 255 \quad (1)$$

where X represents the original feature value and X' denotes the normalized value scaled to the $[0-255]$ range suitable for image representation.

Following prior studies [90, 91, 92, 93], the structured tabular traffic data was transformed into image-based representations to enable compatibility with convolutional neural network architectures. Specifically, consecutive chunks of 180 traffic records were extracted and reshaped into RGB images of dimension $60 \times 60 \times 3$. The first 60 records were mapped to the red channel, the next 60 to the green channel, and the final 60 to the blue channel. Each generated image was assigned the corresponding class label among the 11 DDoS attack categories and benign traffic.

This transformation encodes temporal-spatial traffic behavior patterns into structured visual representations, enabling the use of pre-trained convolutional models for traffic classification.

The dataset was divided into training, validation, and test subsets with 60%, 20%, and 20% splits, respectively. The split was performed stratified to preserve

class distribution across subsets and avoid sampling bias.

4.2 Pre-trained Models Selection

The pre-trained models were selected based on the following criteria:

- The model is designed for image classification within transfer learning frameworks.
- The model is available in TensorFlow/Keras for reproducibility and deployment compatibility.
- The model can accept the transformed image size directly or requires minimal resizing (less than 20% upscale).
- The total number of parameters is below 15 million to align with resource constraints typical in IoT and fog-level deployments.

The use of TensorFlow/Keras facilitates deployment in edge and mobile environments due to its broad industry adoption and support for lightweight inference engines.

Based on these criteria, the selected pre-trained models are summarized in Table 1. The table presents the model characteristics, parameter counts, architectural type, and input handling capability.

4.3 Implementation Specification

The optimization strategy plays a significant role in ensuring stable convergence during fine-tuning. In this study, Stochastic Gradient Descent (SGD) was employed due to its stability and controlled parameter updates in image classification tasks [94, 95].

Table 1: Comparison of selected pre-trained models based on selection criteria.

Model	Model Description	No. Param.	Type	Handle Input Size
MobileNet	Lightweight CNN for mobile devices	4M	Lightweight	Yes
MobileNetV2	Improved MobileNet with depthwise separable convolutions	3.4M	Lightweight	Yes
MobileNetV3	Optimized MobileNet version for efficiency	5.4M	Lightweight	Yes
DenseNet121	Densely connected CNN with fewer parameters	8M	CNN-Based	Yes
DenseNet169	Deeper DenseNet variant	14M	CNN-Based	No
EfficientNet-B0	Optimized for accuracy–efficiency balance	5.3M	Advanced Architecture	No
EfficientNetB1	Larger EfficientNet variant with higher capacity	7.8M	Advanced Architecture	No

Transfer learning with partial fine-tuning was applied by unfreezing the top layers of each model. Since fine-tuning pre-trained networks requires careful learning rate control, the initial learning rate was set to $lr = 0.001$. A Reduce-on-Plateau scheduler was implemented to reduce the learning rate by a factor of 0.5 if validation accuracy did not improve for three consecutive epochs.

All models were trained under identical experimental conditions to ensure fair comparison across architectures. Performance was evaluated on the independent test set using standard classification metrics.

4.4 Experimental Setup

All experiments were implemented in Python using TensorFlow/Keras. The transformed traffic samples were stored and loaded in HDF5 format using the `h5py` library. Each input image was normalized prior to training by scaling pixel values into the $[0,1]$ range via division by 255. Class labels were encoded using one-hot encoding to support multi-class classification across benign traffic and the DDoS categories included in CICDDoS2019.

4.4.1 Data Splitting and Evaluation Protocol

To ensure a fair comparison across architectures, all models were trained and evaluated using the same data-splitting protocol. The dataset was split into training, validation, and test sets using stratified sampling to preserve the class distribution. Specifically, 20% of the full dataset was reserved as a validation set, and from the remaining portion an additional 20% was held out for final testing. This protocol yields an approximate split of 64% for training, 16% for validation, and 20% for

testing. All reported performance metrics, cost measures, and reliability statistics were computed on the held-out test set.

4.4.2 Transfer Learning and Fine-tuning Strategy

We adopted a transfer learning approach using ImageNet-pretrained convolutional neural networks as feature extractors, followed by fine-tuning to adapt the representations to the domain of network traffic images. Each base model was initialized with `include_top=False` and extended with a lightweight classification head for multi-class classification. The classification head consisted of global average pooling, a dense layer with ReLU activation, and a final softmax layer with the number of traffic classes.

To provide a consistent fine-tuning policy across architectures, each pretrained backbone was partially unfrozen by enabling training for the last 20% of its layers while keeping the remaining layers frozen. This design supports domain adaptation while limiting the computational cost and reducing the risk of catastrophic forgetting. The exact number of unfrozen layers, as well as the resulting trainable and non-trainable parameter counts, varies by architecture and is reported explicitly in Table 2. The provided implementation script reflects the MobileNet configuration, while the remaining models follow the same pipeline with the corresponding pretrained backbone substituted and the last 20% layer-unfreezing rule applied.

4.4.3 Training Configuration

All models were trained using categorical cross-entropy loss and the Stochastic Gradient Descent (SGD) opti-

mizer with momentum, as specified earlier. Training was conducted for 30 epochs with a batch size of 32 and an initial learning rate of 0.001. To stabilize convergence during fine-tuning, a ReduceLROnPlateau scheduler was used, reducing the learning rate by a factor of 0.5 when the validation loss failed to improve for three consecutive epochs. This setup was applied consistently across all evaluated architectures to ensure that model comparisons reflect architectural differences rather than training-policy variation.

4.4.4 Cost and Timing Measurement

To quantify computational cost and fog-level feasibility, we recorded both total training time and per-sample inference latency. Training time was measured as the elapsed time required to complete the full training process for each model, and inference latency was computed as the average prediction time per test sample. These measures reflect the practical deployment overhead, including the implied energy cost associated with compute usage, and are reported in Table 3.

4.4.5 Performance and Reliability Measurement

Model performance was evaluated using accuracy, precision, recall, F1-score, and AUC, together with additional security-relevant reliability indicators including Cohen’s kappa and Hamming loss, as reported in Table 4. To further assess detection reliability beyond accuracy, we computed confidence-oriented statistical measures including 95% confidence intervals, Matthews correlation coefficient (MCC), balanced accuracy, log loss, and Youden’s index, reported in Table 5. These measures were used to characterize stability, agreement beyond chance, and robustness under multi-class conditions, which are essential for operational DDoS detection.

4.4.6 Explainability and Reliability Support

Beyond internal confidence statistics, reliability was further examined through post-hoc explainability analysis. Grad-CAM was employed to inspect spatial localization patterns used by each model to support its predicted class, while SHAP was used to quantify feature-attribution contributions. Together, these explainability methods provide complementary evidence that models rely on consistent, interpretable structures within the transformed traffic representations, supporting trust and transparency in security decision-making.

5 Results and Evaluations

In our empirical evaluation, we evaluate the pre-trained models performance, cost, and reliability.

5.1 Cost Evaluation

For cost evaluation, we focus on implementation cost from two perspectives: (i) computational demand, which reflects hardware requirements and energy consumption, and (ii) time cost, which directly affects operational responsiveness. We compared the models based on total training time and average test time per sample, as inference time is a strong indicator of operational latency and energy cost during deployment.

We compared the models for the time required for training and the average test time per sample, which are significant indicators of the energy cost to prepare and execute the models. Table 3 shows the total training time (in minutes) and average test time per sample (in seconds).

5.2 Performance Evaluation

In our empirical study, we measured the models’ performance using multiple metrics. Table 4 shows a comparison between the pretrained models, including accuracy, precision, recall, F1-score, Area under the curve (AUC), standard error (SE), Cohen’s kappa coefficient (κ), and Hamming loss (HL). Cohen’s Kappa (κ) was used to measure the agreement between predicted and true labels beyond chance. Kappa (κ) is calculated by:

$$\kappa = \frac{P_o - P_e}{1 - P_e} \quad (2)$$

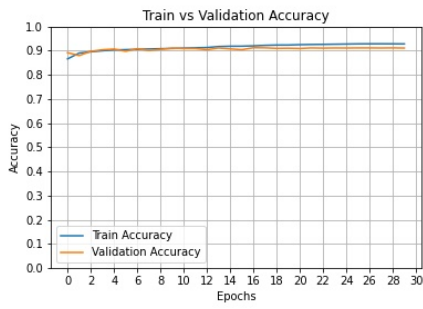
where P_o is the observed agreement (overall accuracy), and P_e is the expected agreement by chance. For multi-class classification:

$$P_o = \sum_{i=1}^K \frac{n_{ii}}{N} \quad (3)$$

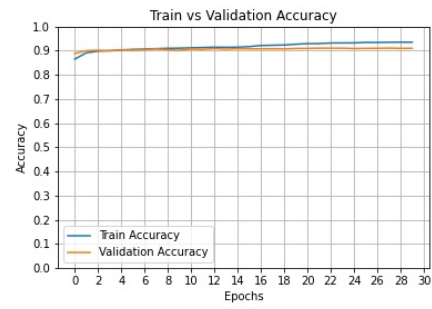
$$P_e = \sum_{i=1}^K \left(\frac{n_{i\cdot}}{N} \times \frac{n_{\cdot i}}{N} \right) \quad (4)$$

where K is the number of classes, N is the total number of samples, n_i total actual samples of class i , $n_{\cdot i}$ is the total predicted samples of class i , and n_{ii} is the correctly classified samples for class i .

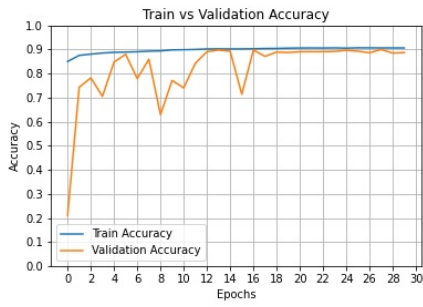
Figure 5 presents the training and validation accuracy curves for all evaluated architectures, illustrated



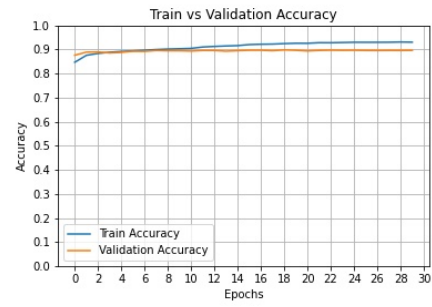
(a) Train versus validation for MobileNet.



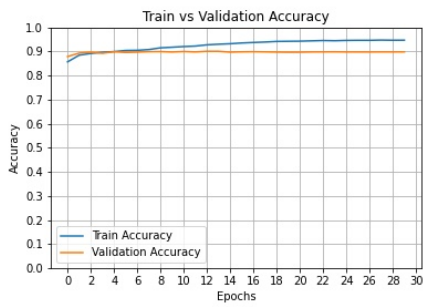
(b) Train versus validation for MobileNetV2.



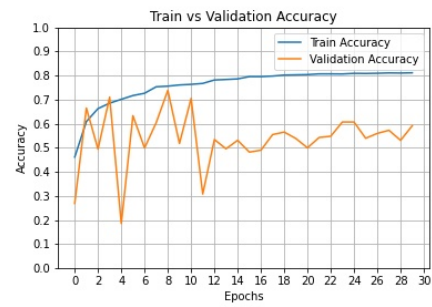
(c) Train versus validation for MobileNetV3.



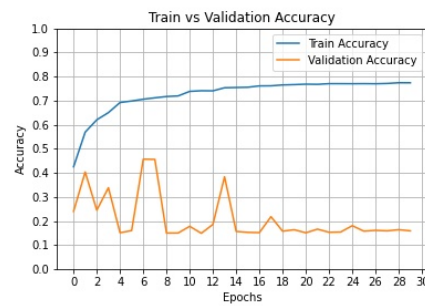
(d) Train versus validation for DenseNet121.



(e) Train versus validation for DenseNet169.



(f) Train versus validation for EfficientNet-B0.



(g) Train versus validation for EfficientNet-B1.

Fig. 5: The train versus validation for the pre-trained models for detecting the DDoS attacks.

Table 2: The fine-tune elements comparison between the selected pre-trained models for the empirical evaluation.

Model	No. Layers	20% Unfreeze	Trainable Param.	Non-trainable Param.
MobileNet	89	17	1,924,404	1,371,840
MobileNetV2	157	33	1,609,164	731,584
MobileNetV3	279	58	2,907,564	1,401,632
DenseNet121	430	88	1,785,548	5,318,336
DenseNet169	598	122	3,780,428	8,969,792
EfficientNet-B0	240	50	2,388,060	1,744,275
EfficientNetB1	342	70	4,229,676	2,428,327

Table 3: A comparison between the pretrained models training and testing time.

Model	Train Time (m)	Avg. test time/sample (s)
MobileNet	61.745	0.000530
MobileNetV2	109.633	0.000864
MobileNetV3	140.915	0.001093
DenseNet121	248.882	0.002191
DenseNet169	345.697	0.003050
EfficientNet-B0	183.157	0.001427
EfficientNetB1	240.622	0.001972

Table 4: A comparison between the pretrained models on DDoS attack detection.

Model	Accuracy	Precision	Recall	F1-Score	AUC (ROC)	SE	Kappa	HL
MobileNet	98.476%	0.90895	0.9008	0.90434	0.94621	0.00163	0.89711	0.09144
MobileNetV2	98.43%	0.9058	0.9058	0.89591	0.94364	0.00166	0.89399	0.0942
MobileNetV3	98.059%	0.89205	0.87209	0.88353	0.93506	0.00182	0.86870	0.11647
DenseNet121	98.25%	0.89142	0.88689	0.88814	0.93863	0.00174	0.88187	0.10498
DenseNet169	98.298%	0.89788	0.89007	0.89788	0.94036	0.00172	0.88509	0.10212
EfficientNet-B0	93.156%	0.58938	0.59623	0.58938	0.77878	0.00279	0.53711	0.41062
EfficientNetB1	85.998%	0.1599	0.21485	0.17463	0.56816	0.00208	0.05826	0.8401

as subfigures for direct comparison. DenseNet121 and DenseNet169 demonstrate stable convergence behavior, with training and validation accuracies increasing steadily and maintaining a minimal generalization gap throughout the epochs. Similarly, MobileNet and MobileNetV3 exhibit consistent learning dynamics, achieving high validation accuracy with only slight divergence from their training performance, indicating strong generalization. In contrast, MobileNetV2 shows greater

variability during early epochs before stabilizing at a lower validation accuracy level. EfficientNet-B0 and EfficientNet-B1 exhibit noticeable fluctuations in validation accuracy across epochs, with larger gaps between training and validation performance, suggesting less stable convergence. Overall, the learning curves indicate that DenseNet-based models achieve the most stable and consistent optimization among the evaluated architectures.

The Receiver Operating Characteristic (ROC) curves for the pre-trained models (Figure 6) demonstrate strong discriminative performance across the twelve traffic classes. For DenseNet121 and DenseNet169, the curves closely approach the upper-left corner of the ROC space, with most class-wise AUC values reaching 1.00 and only minimal deviation for a few categories (e.g., AUC \approx 0.99). Similarly, MobileNet and MobileNetV3 exhibit near-perfect separability for the majority of classes, with AUC values predominantly equal to 1.00 and slight reductions (\approx 0.95–0.99) for specific traffic types. EfficientNet-B0 and EfficientNet-B1 also show strong overall classification performance, with most classes achieving AUC values near 1.00, though minor declines are observed for some categories (\approx 0.95–0.97). In contrast, MobileNetV2 presents comparatively lower performance variability across several classes, with AUC values ranging more broadly (e.g., \approx 0.84–0.99) and one class exhibiting substantially reduced separability. Overall, the ROC curves indicate that most architectures achieve excellent class discrimination, with DenseNet and MobileNetV3 demonstrating the most consistently high AUC values across all traffic categories.

5.3 Confidence Interval Evaluation

Model reliability is evaluated using confidence-oriented statistical measures. Table 5 reports additional analysis, including the 95% confidence interval, Matthews Correlation Coefficient (MCC), balanced accuracy (macro true positive rate), cross-entropy (log loss), and Youden Index. The Matthews Correlation Coefficient (MCC) was employed due to its robustness to class imbalance and its ability to summarize the confusion matrix into a single correlation value. Additionally, Youden’s Index J was calculated to evaluate the overall discriminative power by combining sensitivity and specificity into a single statistic.

For our multi-class classification task, the Multi-Class Generalized (MCC) is calculated by:

$$\text{MCC} = \frac{\sum_k \sum_l \sum_m C_{kk} C_{lm} - C_{kl} C_{mk}}{\sqrt{(\sum_k t_k p_k) (\sum_k t_k n_k) (\sum_k p_k n_k)}} \quad (5)$$

where C is the confusion matrix, C_{kk} is the correct classifications (diagonal elements of the confusion matrix), t_k is the total true instances of class k , p_k is the total predicted instances of class k , and n_k is the total samples not in class k . The Youden index for binary classes is calculated by:

$$J = \text{Sensitivity} + \text{Specificity} - 1 = J = \text{TPR} + \text{TNR} - 1 \quad (6)$$

where the true positive rate (sensitivity) $\text{TPR} = \frac{\text{TP}}{\text{TP} + \text{FN}}$, and the true negative rate (specificity) $\text{TNR} = \frac{\text{TN}}{\text{TN} + \text{FP}}$. In our multiclass task, the Youden Index is calculated by:

$$J_{\text{macro}} = \frac{1}{K} \sum_{i=1}^K (\text{TPR}_i + \text{TNR}_i - 1) \quad (7)$$

where K is the number of classes, TPR_i is the sensitivity of class i , and TNR_i is the specificity of class i .

6 Model Interpretability and Explainability Analysis

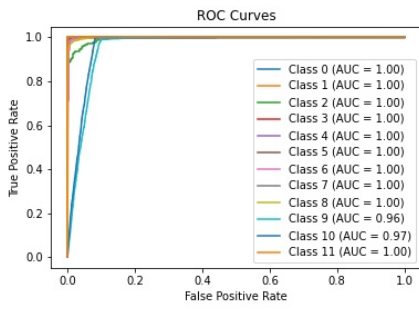
To ensure the reliability and transparency of the proposed pretrained DDoS detection models, an interpretability analysis was conducted using Grad-CAM techniques for spatial localization and SHAP explanations for quantitative feature attribution.

6.1 Grad-CAM Spatial Attention Analysis

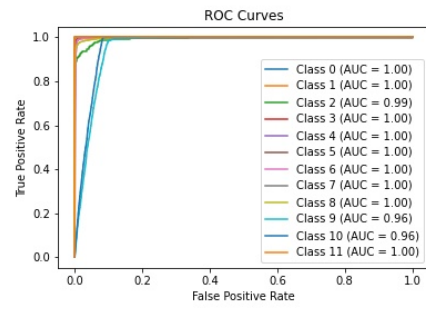
To visualize class-discriminative regions used by each model, Grad-CAM heatmaps (Figure 7) were generated for all twelve traffic categories. The top row of each figure shows the original traffic image, and the bottom row shows the corresponding Grad-CAM heatmap.

DenseNet Architectures As illustrated in Fig. 7d and Fig. 7e, DenseNet121 and DenseNet169 demonstrate highly compact and class-specific activation maps. The models consistently focus on dense vertical packet-structure bands corresponding to attack signatures while suppressing background stripes. DenseNet169 shows slightly stronger activation compactness than DenseNet121, indicating enhanced feature reuse and discriminative amplification due to deeper dense connectivity.

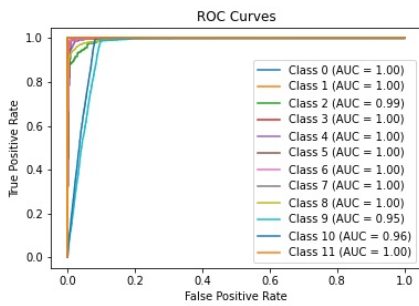
MobileNet Family The Grad-CAM visualizations for the MobileNet family (Figures 7a, 7b, and 7c) show clear differences in spatial attention behavior across the three variants. The original MobileNet exhibits moderate localization capability, with activation maps generally highlighting discriminative vertical packet structures, albeit with noticeable diffusion into adjacent background regions. MobileNetV2 shows comparatively weaker activation intensities and a broader attention distribution, indicating less precise spatial discrimination. In contrast, MobileNetV3 shows improved compactness and consistency of activation patterns, with more concentrated focus on class-relevant regions and reduced background



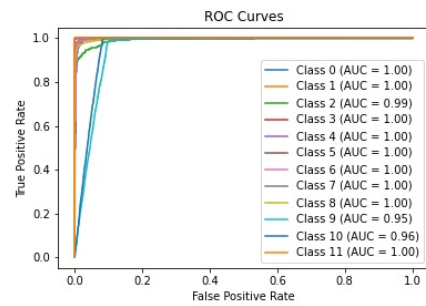
(a) ROC results for MobileNet.



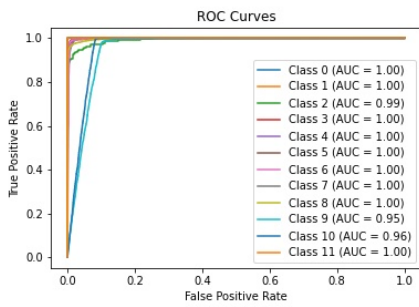
(b) ROC results for MobileNetV2.



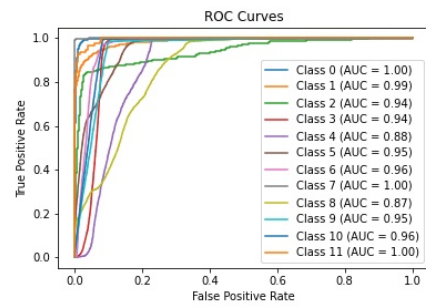
(c) ROC results for MobileNetV3.



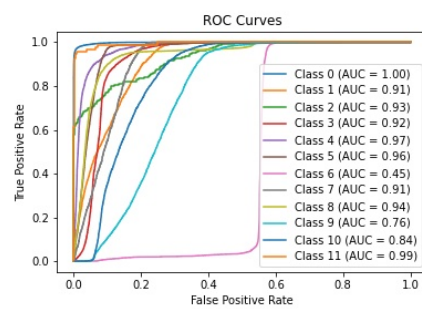
(d) ROC results for DenseNet121.



(e) ROC results for DenseNet169.



(f) ROC results for EfficientNet-B0.



(g) ROC results for EfficientNet-B1.

Fig. 6: The ROC diagrams for the pre-trained models for detecting the DDoS attacks.

Table 5: A statistical analysis comparison between the pretrained models on DDoS attack detection.

Model	95% CI	MCC	Balanced Acc	Log Loss	Youden Index
MobileNet	(0.90536,0.91177)	0.89718	0.9008	3.28369	0.89242
MobileNetV2	(0.90255, 0.90905)	0.89425	0.94364	3.28699	0.88728
MobileNetV3	(0.87997,0.88710)	0.87077	0.93063	3.32906	0.86127
DenseNet121	(0.89161, 0.89843)	0.88212	0.93863	3.28696	0.87726
DenseNet169	(0.89452, 0.90125)	0.88523	0.94036	3.28484	0.88071
EfficientNet-B0	(0.58391, 0.59485)	0.55983	0.77878	2.89804	0.55756
EfficientNetB1	(0.15582, 0.16397)	0.06944	0.56816	5.47480	0.13631

interference. Overall, among the lightweight architectures evaluated, MobileNetV3 achieves the most effective spatial localization and interpretability.

EfficientNet Family The Grad-CAM visualizations in Figures 7f and 7g indicate that the EfficientNet architectures produce comparatively smoother and more spatially diffused activation patterns. While the models successfully identify relevant vertical packet structures associated with attack signatures, the attention maps extend across broader regions, reflecting less concentrated localization. This diffusion is accompanied by weaker suppression of non-informative background areas, suggesting a more distributed evidence aggregation strategy rather than sharp feature discrimination. Among all evaluated models, EfficientNet-B1 exhibits the most widely distributed activation behavior, indicating the lowest degree of spatial compactness and discriminative focus.

As shown in Table 6, DenseNet169 demonstrates the highest spatial compactness and class consistency, whereas EfficientNetB1 exhibits the lowest degree of discriminative localization.

The qualitative categories reported in Table 6 are defined based on visual and structural assessment of the Grad-CAM heatmaps across all twelve classes. Spatial compactness refers to the degree to which activation regions are tightly concentrated around discriminative packet-density structures rather than diffused across adjacent areas. Models categorized as Very High exhibit sharply localized vertical activation bands with minimal spread, whereas models categorized as Low exhibit broad, diffuse attention patterns. Class consistency evaluates the stability of activation behavior across different attack categories. A Very High rating indicates consistent localization patterns across all classes, while Moderate reflects variability in attention precision depending on the attack type. Background suppression measures the model’s ability to avoid activating non-

informative regions (e.g., low-density or blank traffic areas). A Strong rating corresponds to clear suppression of irrelevant regions, whereas Weak indicates noticeable activation outside meaningful packet structures. These categorical assessments are derived from comparative visual inspection of heatmap compactness, intensity concentration, and suppression behavior across all models and classes. The interpretability level is then assigned based on the combined performance across these three criteria.

6.2 SHAP Feature Attribution Analysis

To quantitatively assess the contribution of individual spatial regions to model predictions, SHAP (SHapley Additive exPlanations) values were computed for representative samples from each traffic class. Unlike Grad-CAM, which highlights spatial attention regions, SHAP provides a feature-level attribution score indicating the magnitude and direction of each region’s contribution toward the final class prediction. Positive SHAP values correspond to features that support the predicted class, whereas negative values indicate suppression or counter-evidence. The SHAP visualizations for each evaluated architecture are presented in Figure 8.

DenseNet Architectures As observed in Figure 8d and Figure 8e, the DenseNet architectures exhibit the highest SHAP magnitude range, reaching approximately ± 0.03 . The attribution maps reveal highly concentrated contribution regions aligned with dense vertical packet-structure bands corresponding to attack signatures. Moreover, there is a clear, consistent separation between positive regions that reinforce the predicted attack class and negative regions that suppress non-informative background regions.

This pattern indicates reliance on a decisive feature and strong discriminative capability. The compactness of

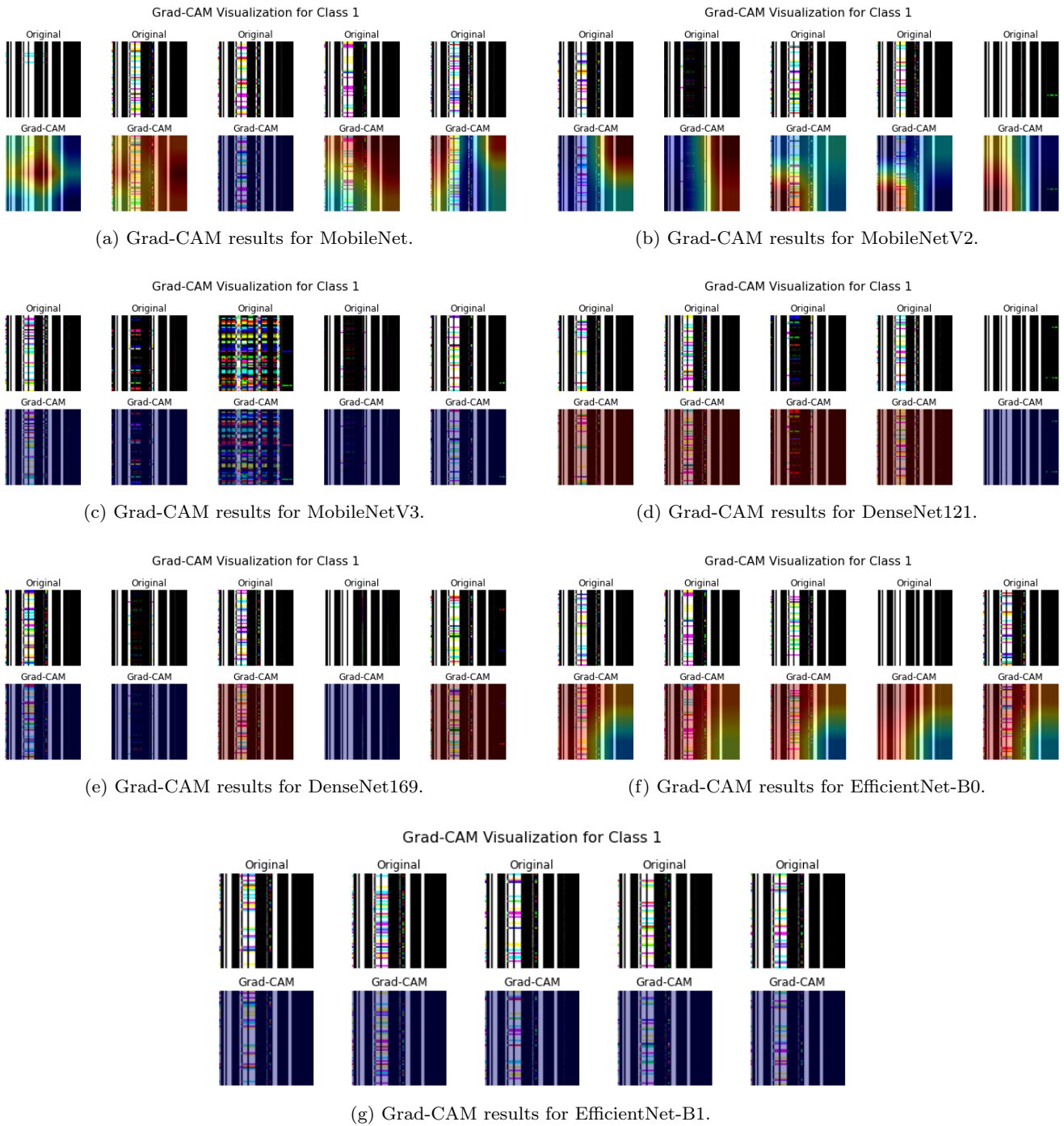


Fig. 7: Grad-CAM heatmaps for the pre-trained models for detecting the DDoS attacks.

SHAP contributions demonstrates that DenseNet models amplify localized, class-specific patterns rather than distributing evidence broadly across the image. Such behavior reflects confident and structured decision-making and aligns with their superior predictive performance.

MobileNet Family Figures 8a, 8b, and 8c show that MobileNet and MobileNetV3 exhibit moderate SHAP

magnitudes, generally around ± 0.02 , while MobileNetV2 displays a lower magnitude range of approximately ± 0.01 . The attribution maps for these models are moderately compact but display some diffusion across adjacent spatial regions.

MobileNetV3 demonstrates improved feature selectivity compared to MobileNetV2, with stronger concentration around discriminative packet structures and

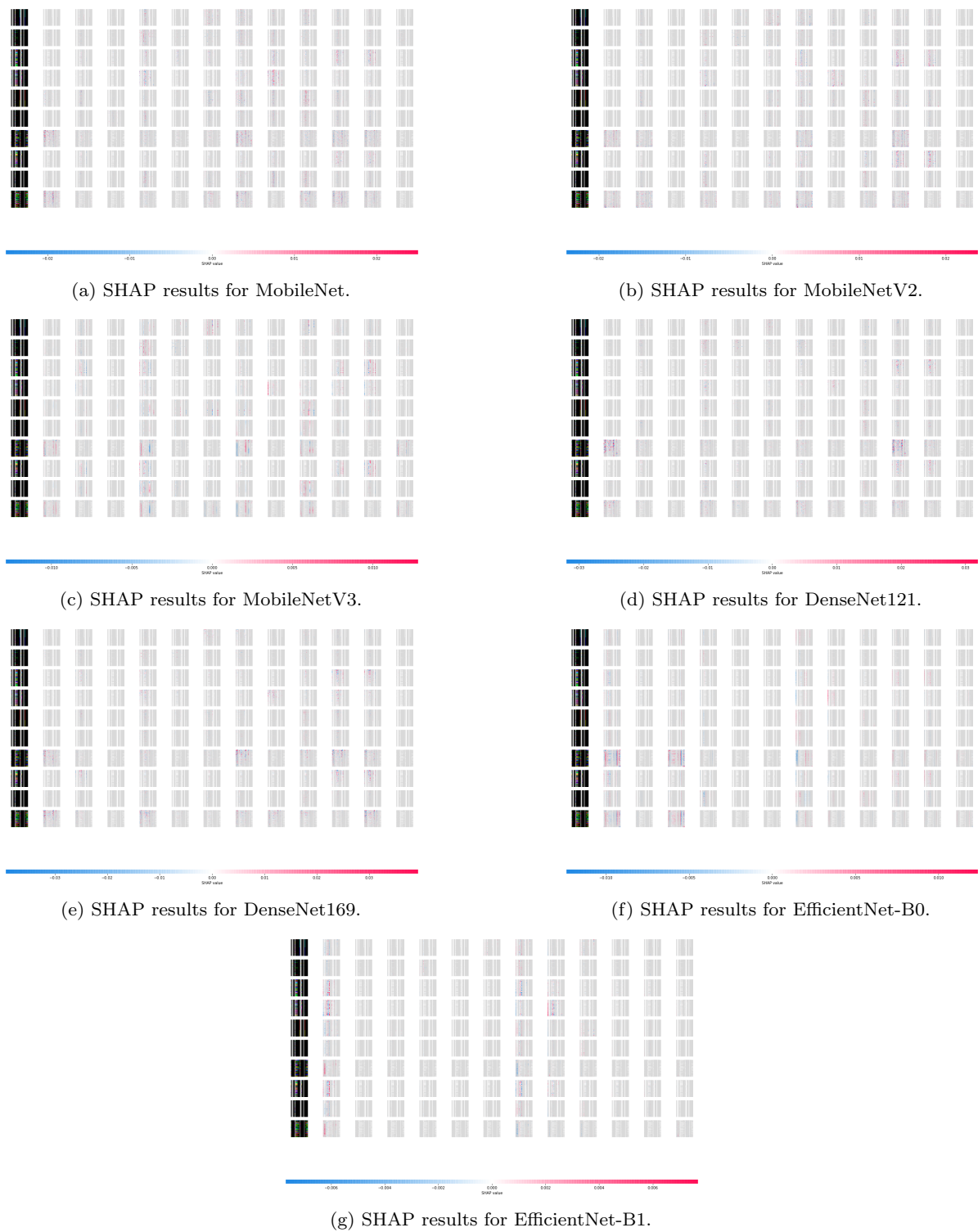


Fig. 8: The SHAP results for the pre-trained models for detecting the DDoS attacks.

Table 6: Grad-CAM Spatial Localization Comparison

Model	Spatial Compactness	Class Consistency	Background Suppression	Interpretability Level
DenseNet169	Very High	Very High	Strong	Excellent
DenseNet121	High	High	Strong	Very Good
MobileNetV3	Moderate to High	Moderate to High	Moderate	Good
MobileNet	Moderate	Moderate	Moderate	Fair–Good
MobileNetV2	Moderate	Moderate	Moderate to Low	Moderate
EfficientNet-B0	Low to Moderate	Moderate	Weak	Moderate
EfficientNet-B1	Low	Moderate	Weak	Limited

clearer suppression of irrelevant regions. In contrast, MobileNetV2 shows weaker attribution intensity and more distributed contribution patterns, indicating less decisive feature usage. Overall, the MobileNet family strikes a balance between computational efficiency and moderate interpretability, with MobileNetV3 being the most interpretable among the lightweight architectures.

EfficientNet Family Figures 8f and 8g illustrate the SHAP attribution behavior of EfficientNet-B0 and EfficientNet-B1. EfficientNet-B0 exhibits moderate magnitude contributions (approximately $+0.02$), but the attribution patterns are noticeably more diffused compared to DenseNet models. Although relevant regions are activated, contributions are distributed across broader spatial areas, suggesting smoother evidence aggregation rather than sharp discriminative emphasis.

EfficientNet-B1 demonstrates the smallest SHAP magnitude range (approximately $+0.006$) among all evaluated models. The attribution maps show highly diffused contributions with limited strong positive or negative peaks. This indicates that the model relies on distributed evidence across many regions rather than concentrating on a few decisive features. While such behavior may enhance generalization stability, it reduces interpretability, clarity, and decisiveness.

Table 7 presents quantitative SHAP attribution characteristics across all evaluated architectures.

6.3 Integrated Interpretability Comparison

The combined Grad-CAM and SHAP analyses demonstrate strong methodological agreement. Architectures that exhibit compact, well-localized spatial attention patterns in Grad-CAM also show higher SHAP magnitudes and clearer positive–negative feature separation. This cross-method consistency strengthens the validity of the interpretability conclusions.

DenseNet169 consistently achieves the highest spatial compactness, the strongest SHAP attribution magnitude, and the most effective background suppression. DenseNet121 follows closely, demonstrating similarly

compact but slightly less intense attribution behavior. MobileNetV3 represents the strongest lightweight architecture in terms of interpretability, while EfficientNet-B1 exhibits the lowest degree of discriminative localization and feature decisiveness.

These interpretability findings align closely with quantitative evaluation metrics such as the Matthews Correlation Coefficient (MCC) and the Youden Index, further reinforcing the relationship between discriminative localization and classification robustness.

Table 8 summarizes the overall interpretability ranking derived from the integrated analysis.

6.4 Class-wise Detection Analysis

To further assess detection reliability across heterogeneous attack categories, confusion matrices were generated for all evaluated architectures. Figure 9 presents the multi-class confusion matrices for the seven pre-trained models under the CICDDoS2019 dataset.

Across the evaluated models, amplification-based attacks such as DNS, NTP, and SSDP exhibit consistently high true-positive rates, as reflected by strong diagonal dominance in the corresponding matrix rows. DenseNet architectures demonstrate the cleanest diagonal concentration with minimal cross-class leakage, indicating stable discrimination across heterogeneous attack categories. MobileNet and MobileNetV3 maintain strong class separation, with limited misclassification, primarily among protocol-based floods that exhibit similar statistical characteristics. In contrast, EfficientNet-B1 shows increased off-diagonal dispersion, reflecting instability in distinguishing certain attack categories and benign traffic. These findings reinforce the reliability metrics reported in Tables 4 and 5.

Results indicate that amplification-style attacks (e.g., DNS, NTP, SSDP) are detected with consistently high true-positive rates, reflecting distinct traffic structures in the image representation. Misclassifications are more likely between traffic classes with similar statistical behavior, particularly between protocol-based floods and

Table 7: SHAP Attribution Comparison Across Architectures

Model	SHAP Magnitude	Attribution Concentration	Negative Suppression	Attribution Strength
DenseNet169	± 0.03	Very Compact	Strong	Very Strong
DenseNet121	± 0.03	Compact	Strong	Strong
MobileNetV3	$\pm 0.02-0.025$	Moderate	Moderate	Moderate-Strong
MobileNet	± 0.02	Moderate	Moderate	Moderate
EfficientNet-B0	± 0.02	Diffused	Moderate-Weak	Moderate
MobileNetV2	± 0.01	Less Compact	Moderate-Weak	Weak-Moderate
EfficientNet-B1	± 0.006	Highly Diffused	Weak	Weak

Table 8: Overall Interpretability Ranking Based on Grad-CAM and SHAP Analysis

Model	Rank
DenseNet169	1
DenseNet121	2
MobileNetV3	3
MobileNet	4
EfficientNet-B0	5
MobileNetV2	6
EfficientNet-B1	7

benign traffic, suggesting overlapping visual patterns in the transformed feature space.

6.5 Implications for Cybersecurity Deployment

Interpretability plays a critical role in intrusion detection systems, particularly in cybersecurity contexts where both false positives and false negatives can have significant operational consequences. Models that exhibit compact spatial localization and decisive feature attribution provide clearer justification for detection decisions and improve system transparency.

DenseNet architectures demonstrate superior explainability through both concentrated Grad-CAM localization and strong SHAP contribution magnitude. Such behavior indicates structured and confident decision-making, which is desirable in security-sensitive environments where auditability and trust are essential. In contrast, architectures exhibiting diffused attribution patterns may still perform adequately but offer less transparent reasoning pathways.

Consequently, from an explainability and deployment perspective, DenseNet-based architectures appear more suitable for real-world DDoS detection systems requiring interpretable and defensible decision-making processes.

7 Discussion

In this section, we synthesize the empirical findings across detection performance, computational cost, reliability metrics, and model interpretability, with emphasis on practical deployment for IoT-driven systems and fog-level intrusion detection. The evaluation spans three architecture families (MobileNet, DenseNet, EfficientNet). It integrates conventional performance metrics (Table 4), computational cost indicators (Table 3), reliability-oriented statistics (Table 5), and explainability evidence from Grad-CAM and SHAP analyses (Figures 7 and 8, Tables 6 and 7).

7.1 Performance Trade-offs Across Architectures

Across the evaluated architectures, MobileNet, DenseNet121, and DenseNet169 achieve consistently high overall accuracy (approximately 98%) and strong macro-level performance (Table 4), indicating that transfer learning on image-encoded network traffic captures discriminative structure for multi-class DDoS recognition. Among these, MobileNet attains the highest reported accuracy (98.476%), whereas DenseNet169 maintains comparable accuracy (98.298%) with strong agreement statistics (Kappa ≈ 0.885) and robust correlation-based reliability (MCC ≈ 0.885 ; Table 5). These results suggest that DenseNet connectivity offers a favorable inductive bias for exploiting repeated packet-structure patterns introduced by the tabular-to-image transformation (Figure 4).

In contrast, EfficientNet architectures underperform in this setting, especially EfficientNet-B1, which exhibits a marked drop in accuracy (85.998%), low agreement (Kappa ≈ 0.058), weak MCC (0.069), and high Hamming loss (0.8401; Table 4). This indicates that despite EfficientNet’s reputation for accuracy–efficiency trade-offs in natural image recognition, it does not transfer robustly to the highly structured, synthetic-like texture patterns represented in network traffic images under the

current fine-tuning scheme. EfficientNet-B0 performs better than B1 but remains substantially lower than MobileNet and DenseNet models, with reduced precision/recall and lower discriminative capacity (AUC \approx 0.779; Table 4).

7.2 ROC Behavior and Class-wise Separability

The ROC subfigures in Figure 6 corroborate the above findings at the class level. DenseNet121 and DenseNet169 display curves that closely approach the upper-left corner for most classes, with class-wise AUC values near 1.00 and limited degradation for only a small subset of categories. MobileNet and MobileNetV3 similarly show near-perfect separability for most classes, with only minor AUC declines (approximately 0.95–0.99) for a few traffic types. These patterns imply strong separability of the learned representations across attack categories under the proposed image encoding.

MobileNetV2 shows greater variability in class-wise AUC values and includes at least one category with noticeably reduced separability, aligning with its slightly weaker macro-level results and reduced explainability coherence. EfficientNet-B0 and EfficientNet-B1 exhibit greater class-dependent deviations, suggesting that the learned evidence for some classes is either less discriminative or more unstable in feature attribution, a claim further supported by the interpretability results discussed later.

7.3 Training Dynamics and Generalization Stability

The train-versus-validation learning curves (Figure 5) provide complementary evidence about optimization stability and generalization. DenseNet121 and DenseNet169 exhibit smooth convergence and a small, stable generalization gap across epochs, indicating consistent optimization and robust generalization under the selected fine-tuning strategy. MobileNet and MobileNetV3 similarly converge steadily with high validation accuracy and limited divergence from training behavior, suggesting that these architectures generalize effectively while maintaining computational efficiency.

In contrast, EfficientNet-B0 and EfficientNet-B1 display noticeable validation oscillations and larger train-validation gaps. Such instability is consistent with their lower performance and reliability statistics (Tables 4 and 5) and suggests sensitivity to hyperparameters, fine-tuning depth, or mismatch between pretraining priors and the target domain. MobileNetV2 also shows higher early-epoch variability before stabilization, which may

partially explain its weaker discriminative and interpretability behavior relative to MobileNetV3.

7.4 Cost and Efficiency for Fog-level Deployment

From a deployment perspective, the cost evaluation demonstrates a clear trade-off between latency and accuracy across the model families. MobileNet achieves the lowest inference time per sample (0.000530 s), followed by MobileNetV2 and MobileNetV3 (Table 3), making MobileNet variants highly attractive for resource-constrained IoT/fog nodes. DenseNet models, while robust and explainable, exhibit higher inference time (DenseNet169: 0.003050 s), reflecting the computational overhead of deeper dense connectivity. EfficientNet-B0 and EfficientNet-B1 fall between MobileNet and DenseNet in inference time, but their performance and reliability limitations reduce their practical suitability under strict operational constraints.

Training time also varies substantially, with MobileNet requiring roughly 62 minutes and DenseNet169 requiring approximately 346 minutes (Table 3). While training costs may be amortized in many deployment scenarios, they become more important in scenarios with frequent model updates, online adaptation, or edge personalization. Therefore, a pragmatic deployment strategy may involve selecting MobileNetV3 when low latency is critical, and selecting DenseNet169 when interpretability and reliability are prioritized.

7.5 Reliability Metrics and Decision Confidence

These reliability gaps are important in operational IoT environments because risk is not determined solely by average accuracy. The reliability-oriented statistics in Table 5 strengthen the interpretation of the performance results. Models with high MCC and Youden Index provide more trustworthy multi-class decision behavior, particularly under uneven class distributions. DenseNet169 and MobileNet achieve strong MCC values near 0.885–0.897 and high Youden Index values near 0.88–0.89, supporting their suitability for operational deployment. In contrast, EfficientNet-B1 demonstrates extremely low MCC and Youden Index values, indicating unreliable class discrimination and weak sensitivity–specificity balance under the evaluated conditions.

These reliability gaps are important in operational environments because operational risk is not governed solely by average accuracy. A model that appears accurate but has weak MCC/Youden scores can still systematically fail for certain critical attack categories, leading to service disruption or undetected intrusions.

7.6 Explainability: Agreement Between Grad-CAM and SHAP

A core contribution of this work is the explainability-aware evaluation of transfer learning architectures for DDoS detection. The Grad-CAM results (Figure 7 and Table 6) show that DenseNet architectures produce the most compact and class-consistent spatial localization patterns, with strong background suppression. MobileNetV3 demonstrates improved compactness compared to MobileNetV2 and the base MobileNet, supporting its role as the most interpretable lightweight model. EfficientNet architectures, particularly EfficientNet-B1, show the most diffuse attention with weaker suppression of non-informative regions, indicating less discriminative localization.

The SHAP analysis (Figure 8 and Table 7) quantitatively confirms these trends. DenseNet models achieve the highest attribution magnitude (approximately ± 0.03) with compact contributions and clear positive-negative separation, reflecting decisive feature reliance and structured evidence. MobileNetV3 exhibits moderate-to-strong attribution magnitude (approximately ± 0.02 – 0.025) with improved selectivity relative to MobileNetV2, while EfficientNet-B1 shows the smallest magnitude (approximately ± 0.006) and highly diffused attribution, indicating weaker decisiveness and less transparent decision logic.

Importantly, the agreement between Grad-CAM (spatial localization) and SHAP (feature attribution magnitude and direction) strengthens confidence in the interpretability conclusions. Models that are compact and consistent in Grad-CAM also exhibit stronger and more separable SHAP patterns, which aligns with the integrated interpretability ranking (Table 8). This multi-method agreement is a practical indicator of trustworthiness: a model that is both accurate and explainable is more suitable for security-sensitive adoption where analysts require defensible explanations.

7.7 Implications for IoT-driven Business Systems

For IoT-driven business systems, the choice of model depends on the balance between operational constraints and trust requirements. Lightweight MobileNet models minimize latency and are well-suited for fog/edge deployment where rapid filtering and early warning are required. Within this family, MobileNetV3 offers a strong compromise, providing high performance and more coherent explanations than MobileNetV2. DenseNet models, particularly DenseNet169, provide the strongest evidence of interpretability and reliability, making them suitable for scenarios where decisions must be auditable

and defensible (e.g., regulated infrastructures, critical services, or environments requiring forensic analysis).

EfficientNet architectures are less favorable in the evaluated configuration due to reduced stability, weaker reliability, and lower interpretability clarity. This does not imply that EfficientNet is inherently unsuitable for cybersecurity, but rather that the architectural priors and fine-tuning configuration may require further adaptation for traffic-image representations (e.g., alternative unfreezing strategies, stronger regularization, or architecture-specific preprocessing).

Overall, the results support a deployment-centric recommendation: MobileNetV3 is a practical choice for low-latency edge detection, whereas DenseNet169 is a strong choice for reliability-critical and interpretability-critical detection pipelines where analyst trust and decision transparency are central requirements.

8 Security Robustness and Limitations

While the proposed evaluation demonstrates strong detection performance across multiple DDoS categories, several security-related limitations should be considered.

First, the evaluation is conducted using the CICDDoS2019 benchmark dataset. Although comprehensive, real-world deployments may encounter unseen attack patterns, distribution shifts, or zero-day attack variants that could impact model generalization.

Second, this study assumes a closed-world setting where attack categories are known during training. The detection capability against novel or adversarially modified attacks remains an open research challenge.

Third, the framework does not explicitly evaluate adversarial evasion techniques such as traffic perturbation or adversarial feature manipulation. Future work may explore adversarial robustness and online adaptive learning mechanisms.

Finally, encrypted traffic environments and payload obfuscation may alter feature distributions, potentially affecting detection reliability.

Despite these limitations, the presented evaluation provides a structured security assessment of pre-trained models under realistic IoT deployment constraints.

9 Conclusion

This paper presented a comprehensive empirical evaluation of transfer learning architectures for DDoS detection in IoT-driven business systems, emphasizing not only predictive performance but also computational cost, reliability, and explainability. Using the CICDDoS2019

benchmark and an image-based transformation of network traffic, seven pretrained models were fine-tuned and compared under a unified experimental protocol.

The results demonstrate that MobileNet- and DenseNet-based architectures achieve strong multi-class detection performance (approximately 98% accuracy), with high agreement and reliability indicators, including Cohen’s Kappa, MCC, and Youden Index. DenseNet169 emerges as the most reliable and explainable architecture, exhibiting compact, class-consistent Grad-CAM localization and the strongest SHAP attribution magnitudes, with clear positive-negative separation. MobileNetV3 represents the strongest lightweight alternative, providing high detection capability with improved interpretability coherence compared to MobileNetV2, while also maintaining low inference latency suitable for fog/edge deployment. In contrast, EfficientNet-B0 and especially EfficientNet-B1 exhibit reduced stability, weaker reliability statistics, and more diffuse interpretability patterns under the evaluated configuration, limiting their suitability for resource-constrained and security-sensitive deployment.

From a practical deployment perspective, the findings highlight an actionable trade-off. For real-time fog-level detection under strict latency and resource constraints, MobileNetV3 provides an effective balance between efficiency and explainability. For environments where decision accountability and analyst trust are critical, DenseNet169 delivers the most defensible, transparent detection behavior. Collectively, the evidence suggests that interpretability measures are not merely auxiliary; instead, compact localization and decisive attribution align with stronger reliability metrics and support higher-confidence intrusion detection in operational business systems.

Future work will extend this study by incorporating deeper, confusion-matrix-driven class-specific error analysis, evaluating robustness under distribution shifts (e.g., unseen attack variants), and exploring edge-aware compression and quantization strategies to reduce inference cost further while preserving interpretability and reliability guarantees.

Credit Authorship Contribution Statement

Nelly Elsayed (sole author): Conceptualization, Methodology, Data Curation, Formal Analysis, Investigation, Visualization, Writing, and Original Draft Preparation, Validation, Project Administration, Writing, Review and Editing.

Declaration of competing interest

The authors declare that they have no competing financial or personal interests that could have influenced the work reported in this paper.

Funding

This research did not receive any specific grant from funding agencies in the public, commercial, or not-for-profit sectors.

Data availability

The dataset CIC-DDoS2019 Dataset that has been used in this paper is publicly available at the following links:

- <https://data.mendeley.com/datasets/ssnc74xm6r/1>
- <https://www.unb.ca/cic/datasets/ddos-2019.html>

The image format of this dataset is publicly available but requires membership to access using the IEEE DataPort the following link:

- <https://ieee-dataport.org/documents/iot-dos-and-ddos-attack-dataset>

Declaration of generative AI and AI-assisted technologies in the writing process

During the preparation of this work, the authors used generative AI including ChatGPT, Grammarly, and Gemini tools solely for language refinement to ensure that the texts are free of errors in grammar, spelling, and punctuation. In addition to LaTeX formatting assistance. All generated text was thoroughly reviewed, edited, and verified by the authors, who take full responsibility for the content and integrity of the final manuscript.

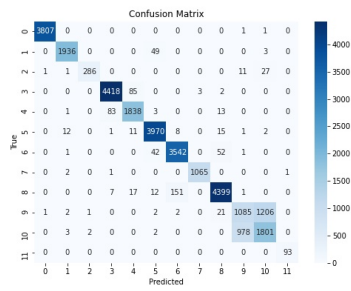
References

1. E. Ebrahimpour, S. Babaie, *International Journal of Information Security* **23**(3), 1583 (2024)
2. F.A. Alaba, M. Othman, I.A.T. Hashem, F. Alotaibi, *Journal of network and computer applications* **88**, 10 (2017)
3. T. Kotsiopoulos, P. Radoglou-Grammatikis, Z. Lekka, V. Mladenov, P. Sarigiannidis, *International Journal of Information Security* **24**(4), 157 (2025)

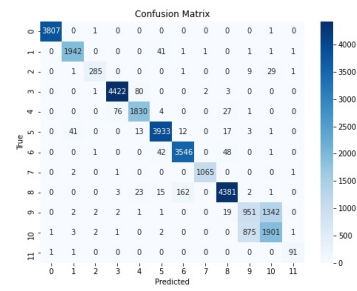
4. I. Behnke, H. Austad, *IEEE Internet of Things Journal* **11**(5), 7399 (2023)
5. R. Reyes-Acosta, C. Dominguez-Baez, R. Mendoza-Gonzalez, M. Vargas Martin, *International Journal of Information Security* **24**(1), 31 (2025)
6. S. Selvaraj, S. Sundaravaradhan, *SN Applied Sciences* **2**(1), 139 (2020)
7. Z. ElSayed, M. Ozer, N. Elsayed, A. Abdelgawad, arXiv preprint arXiv:2305.19347 (2023)
8. M.A. Azzawi, R. Hassan, K.A.A. Bakar, *International Journal of Applied Engineering Research* **11**(20), 10216 (2016)
9. L. Jayashree, G. Selvakumar, in *Getting Started with Enterprise Internet of Things: Design Approaches and Software Architecture Models* (Springer, 2020), pp. 71–96
10. W. Wijesundara, J.S. Lee, D. Tith, E. Aloupogianni, H. Suzuki, T. Obi, *International Journal of Information Security* **23**(3), 1927 (2024)
11. S.S.I. Samuel, in *2016 3rd MEC International conference on big data and smart city (ICBDSC)* (IEEE, 2016), pp. 1–4
12. M. Alaa, A.A. Zaidan, B.B. Zaidan, M. Talal, M.L.M. Kiah, *Journal of network and computer applications* **97**, 48 (2017)
13. N.B. Jones, C.M. Graham, *Bulletin of Science, Technology & Society* **38**(1-2), 3 (2018)
14. Y.S. Jeong, *Journal of Convergence for Information Technology* **7**(2), 83 (2017)
15. K. Shetty, M. Mudholkar, P. Mudholkar, M. LB, S. TN, et al., in *2024 Second International Conference Computational and Characterization Techniques in Engineering & Sciences (IC3TES)* (IEEE, 2024), pp. 1–5
16. Y.Y. Shaheen, M.J. Hornos, C. Rodríguez-Domínguez, *International Journal of Information Security* **24**(6), 236 (2025)
17. I. Nappi, G. de Campos Ribeiro, *Journal of Corporate Real Estate* **22**(1), 71 (2020)
18. P. Sun, Y. Wan, Z. Wu, Z. Fang, Q. Li, *Computers & Security* **148**, 104097 (2025)
19. R. Vishwakarma, A.K. Jain, *Telecommunication systems* **73**(1), 3 (2020)
20. L. Dzamesi, N. Elsayed, in *2025 IEEE 4th International Conference on Computing and Machine Intelligence (ICMI)* (IEEE, 2025), pp. 01–08
21. CISCO. What is a ddos attack? (2025). URL <https://www.cisco.com/c/en/us/products/security/what-is-a-ddos-attack.html>. Accessed: 19 February 2025
22. Z. ElSayed, A. Abdelgawad, N. Elsayed, arXiv preprint arXiv:2501.18549 (2025)
23. L.F. Eliyan, R. Di Pietro, *Future Generation Computer Systems* **122**, 149 (2021)
24. E. Džaferović, A. Sokol, A. Abd Almisreb, S.M. Norzeli, *Sustainable Engineering and Innovation* **1**(1), 43 (2019)
25. National Cybersecurity Center of Excellence (NC-CoE) and National Institute of Standards and Technology (NIST). NIST Special Publication 1800-26A: Data Integrity: Detecting and Responding to Ransomware and Other Destructive Events, Volume A: Executive Summary. <https://www.nccoe.nist.gov/publication/1800-26/VolA/1800-26A.html> (2020)
26. S. Samonas, D. Coss, *Journal of Information System Security* **10**(3) (2014)
27. VERCARA. Vercara ddos analysis reports (2024). URL <https://vercara.com/resources/reports>. Accessed: 19 February 2025
28. P. Kumari, A.K. Jain, *Computers & Security* **127**, 103096 (2023)
29. J. Yan, H. Zhou, W. Wang, *Information Systems Frontiers* pp. 1–20 (2025)
30. Y. Al-Hadhrami, F.K. Hussain, *World Wide Web* **24**(3), 971 (2021)
31. D.M. Sharif, H. Beitollahi, *Computers & Security* **135**, 103511 (2023)
32. E. Alomari, S. Manickam, B.B. Gupta, S. Karuppayah, R. Alfaris, arXiv preprint arXiv:1208.0403 (2012)
33. N. Elsayed, Z. ElSayed, M. Bayoumi, in *2023 IEEE World AI IoT Congress (AIIoT)* (IEEE, 2023), pp. 0134–0142
34. N. Pandey, P.K. Mishra, *Computers & Security* **150**, 104199 (2025)
35. N. Hoque, D.K. Bhattacharyya, J.K. Kalita, *IEEE Communications Surveys & Tutorials* **17**(4), 2242 (2015)
36. F. Brezo, I. Santos, P.G. Bringas, J.L. del Val, in *2011 22nd International Workshop on Database and Expert Systems Applications* (IEEE, 2011), pp. 95–101
37. T. Al-Shurbaji, M. Anbar, S. Manickam, I.H. Hasbullah, N. Alfriehat, B.A. Alabsi, A.R. Alzighaibi, H. Hashim, *IEEE Access* **13**, 11792 (2025)
38. I. Sharafaldin, A.H. Lashkari, S. Hakak, A.A. Ghorbani, in *2019 international carnahana conference on security technology (ICCST)* (IEEE, 2019), pp. 1–8
39. B.A. Khalaf, S.A. Mostafa, A. Mustapha, M.A. Mohammed, W.M. Abdullallah, *IEEE Access* **7**, 51691 (2019)
40. S. Ghazanfar, F. Hussain, A.U. Rehman, U.U. Fayyaz, F. Shahzad, G.A. Shah, in *2020 International Conference on Emerging Trends in Smart*

- Technologies (ICETST)* (IEEE, 2020), pp. 1–6
41. R. Doshi, N. Apthorpe, N. Feamster, in *2018 IEEE security and privacy workshops (SPW)* (IEEE, 2018), pp. 29–35
 42. Z.S. Zaghoul, N. Elsayed, C. Li, M. Bayoumi, in *2021 IEEE 7th World Forum on Internet of Things (WF-IoT)* (IEEE, 2021), pp. 628–632
 43. W. Almobaideen, O. Abu Alghanam, M. Abdullah, S.B. Hussain, U. Alam, *International Journal of Information Security* **24**(3), 110 (2025)
 44. N. Elsayed, L. Dzamesi, Z. ElSayed, M. Ozer, arXiv preprint arXiv:2507.05132 (2025)
 45. S.M. Doğan, A. Koçak, M. Alkan, *International Journal of Information Security* **24**(5), 209 (2025)
 46. S. Kaur, A.K. Sandhu, A. Bhandari, *International Journal of Information Security* **22**(6), 1949 (2023)
 47. N. Elsayed, Z. ElSayed, A. Abdelgawad, in *The International FLAIRS Conference Proceedings*, vol. 38 (2025), vol. 38
 48. M. Mittal, K. Kumar, S. Behal, *Soft computing* **27**(18), 13039 (2023)
 49. S. Hizal, U. Cavusoglu, D. Akgun, *Internet of Things* **28**, 101336 (2024)
 50. M. Roopak, G.Y. Tian, J. Chambers, in *2020 10th annual computing and communication workshop and conference (CCWC)* (IEEE, 2020), pp. 0562–0567
 51. A. Agrawal, P. Baniya, E.M. Alazzawi, N. Rakesh, B. Bhushan, A. Jamil, in *2024 2nd International Conference on Artificial Intelligence, Blockchain, and Internet of Things (AIBThings)* (IEEE, 2024), pp. 1–5
 52. V.E. Quincozes, S.E. Quincozes, J.F. Kazienko, S. Gama, O. Cheikhrouhou, A. Koubaa, *International Journal of Information Security* **23**(3), 1975 (2024)
 53. Z. ElSayed, N. Elsayed, C. Li, M. Bayoumi, in *2022 IEEE 8th World Forum on Internet of Things (WF-IoT)* (IEEE, 2022), pp. 1–5
 54. R. Alenezi, S.A. Ludwig, in *2021 IEEE symposium series on computational intelligence (SSCI)* (IEEE, 2021), pp. 01–10
 55. F. Tempel, D. Groos, E.A.F. Ihlen, L. Adde, I. Strümke, *Applied Intelligence* **55**(17), 1107 (2025)
 56. M. Tatam, B. Shanmugam, S. Azam, K. Kannoorpatti, *Heliyon* **7**(1), e05969 (2021). DOI 10.1016/j.heliyon.2021.e05969. URL <https://linkinghub.elsevier.com/retrieve/pii/S2405844021000748>
 57. G. Apruzzese, M. Andreolini, L. Ferretti, M. Marchetti, M. Colajanni, *Digital Threats: Research and Practice* **3**(3), 1–19 (2022). DOI 10.1145/3469659. URL <https://dl.acm.org/doi/10.1145/3469659>
 58. T. Böttger, L. Braun, O. Gasser, F. Von Eye, H. Reiser, G. Carle, in *International Workshop on Traffic Monitoring and Analysis* (Springer, 2015), pp. 205–218
 59. M. Antonakakis, T. April, M. Bailey, M. Bernhard, E. Bursztein, J. Cochran, Z. Durumeric, J.A. Halderman, L. Invernizzi, M. Kallitsis, D. Kumar, C. Lever, Z. Ma, J. Mason, D. Menscher, C. Seaman, N. Sullivan, K. Thomas, Y. Zhou, in *Proceedings of the 26th USENIX Security Symposium* (2017), pp. 1093–1110
 60. C. Rossow, *Proceedings of the Network and Distributed System Security Symposium (NDSS)* (2014)
 61. J. Mirkovic, P. Reiher, *ACM SIGCOMM Computer Communication Review* **34**(2), 39 (2004)
 62. Z. Durumeric, E. Wustrow, J.A. Halderman, *Proceedings of the Network and Distributed System Security Symposium (NDSS)* (2015)
 63. C. Kolias, G. Kambourakis, A. Stavrou, J. Voas, *Computer* **50**(7), 80 (2017)
 64. B. Biggio, F. Roli, *Pattern Recognition* **84**, 317 (2018)
 65. C.M. Giattino, L. Kwong, C. Rafetto, N.A. Farahany, in *Proceedings of the 2019 AAAI/ACM Conference on AI, Ethics, and Society* (ACM, Honolulu HI USA, 2019), p. 397–402. DOI 10.1145/3306618.3314269. URL <https://dl.acm.org/doi/10.1145/3306618.3314269>
 66. I. Stojmenovic, S. Wen, *Proceedings of the 2014 Federated Conference on Computer Science and Information Systems* pp. 1–8 (2014)
 67. S. Yi, C. Li, Q. Li, *Proceedings of the 2015 Workshop on Mobile Big Data* pp. 37–42 (2015)
 68. T.T. Nguyen, G. Armitage, *IEEE Communications Surveys & Tutorials* **10**(4), 56 (2008). DOI 10.1109/SURV.2008.080406
 69. A.W. Moore, D. Zuev, *ACM SIGMETRICS Performance Evaluation Review* **33**(1), 50 (2005)
 70. S. García, M. Grill, J. Stiborek, A. Zumino, *Computers & Security* **45**, 100 (2014). DOI <https://doi.org/10.1016/j.cose.2014.05.011>. URL <https://www.sciencedirect.com/science/article/pii/S0167404814000923>
 71. R. Sommer, V. Paxson, in *2010 IEEE Symposium on Security and Privacy* (2010), pp. 305–316. DOI 10.1109/SP.2010.25
 72. S. Axelsson, *Technical Report*, Chalmers University (2000)
 73. M. Tavallaee, E. Bagheri, W. Lu, A.A. Ghorbani, in *2009 IEEE Symposium on Computational Intelligence for Security and Defense Applications* (2009), pp. 1–6. DOI 10.1109/CISDA.2009.5356528

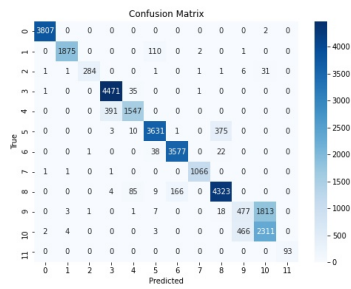
74. M.A. Jabraeil Jamali, B. Bahrami, A. Heidari, P. Allahverdizadeh, F. Norouzi, M.A. Jabraeil Jamali, B. Bahrami, A. Heidari, P. Allahverdizadeh, F. Norouzi, Towards the Internet of Things: Architectures, Security, and Applications pp. 9–31 (2020)
75. F. Olivier, G. Carlos, N. Florent, *Procedia Computer Science* **52**, 1028 (2015)
76. S.W. Azumah, N. Elsayed, V. Adewopo, Z.S. Zaghoul, C. Li, in *2021 IEEE 7th World Forum on Internet of Things (WF-IoT)* (IEEE, 2021), pp. 836–841
77. H.F. Atlam, G.B. Wills, Digital twin technologies and smart cities pp. 123–149 (2020)
78. X. Li, Q. Wei, Z. Wu, W. Guo, in *Proceedings of the 2023 2nd International Conference on Networks, Communications and Information Technology* (ACM, Qinghai China, 2023), p. 35–41. DOI 10.1145/3605801.3605808. URL <https://dl.acm.org/doi/10.1145/3605801.3605808>
79. M. Conti, A. Dehghantanha, K. Franke, S. Watson, *Future Generation Computer Systems* **78**, 544 (2018)
80. (Prentice Hall Professional Technical Reference, Upper Saddle River, N.J, 2005)
81. S.M. Specht, R.B. Lee, *Proceedings of the International Workshop on Security in Parallel and Distributed Systems* (2004)
82. J. Czyz, K. Allman, J. Zhang, E. Osterweil, M. Bailey, M. Karir, in *Proceedings of the 2014 ACM Conference on Internet Measurement Conference (IMC)* (2014)
83. M.J. Farooq, Q. Zhu, *IEEE Transactions on Information Forensics and Security* **14**(9), 2412 (2019). DOI 10.1109/TIFS.2019.2898817
84. B. Bala, S. Behal, *Computer science review* **52**, 100631 (2024)
85. S. Kaur, K. Kumar, N. Aggarwal, G. Singh, *Computers & Security* **110**, 102423 (2021)
86. A. Sanmorino, H. Di Kesuma, *Bulletin of Electrical Engineering and Informatics* **13**(2), 1362 (2024)
87. A. Sanmorino, L. Marnisah, H. Di Kesuma, *Engineering, Technology & Applied Science Research* **14**(5), 16444 (2024)
88. A. Kachavimath, S. Vaishyar, A. Chugani, S. Joshi, S.A. More, G. Narayan, in *International Conference on Data Science and Applications* (Springer, 2025), pp. 13–23
89. G. Somani, M.S. Gaur, D. Sanghi, M. Conti, R. Buyya, *Computer communications* **107**, 30 (2017)
90. X. Liu, Z. Tang, B. Yang, in *2019 IEEE 5th Intl Conference on Big Data Security on Cloud (Big-DataSecurity), IEEE Intl Conference on High Performance and Smart Computing (HPSC) and IEEE Intl Conference on Intelligent Data and Security (IDS)* (IEEE, 2019), pp. 61–66
91. F. Hussain, S.G. Abbas, M. Husnain, U.U. Fayyaz, F. Shahzad, G.A. Shah, in *2020 IEEE 23rd International Multitopic Conference (INMIC)* (IEEE, 2020), pp. 1–6
92. W. Liu, X. Liu, X. Di, H. Qi, in *2019 1st international conference on Industrial Artificial Intelligence (IAI)* (IEEE, 2019), pp. 1–6
93. Z. Li, Z. Qin, K. Huang, X. Yang, S. Ye, in *International conference on neural information processing* (Springer, 2017), pp. 858–866
94. S. Klein, J.P. Pluim, M. Staring, M.A. Viergever, *International journal of computer vision* **81**, 227 (2009)
95. E.M. Dogo, O. Afolabi, N. Nwulu, B. Twala, C. Aigbavboa, in *2018 international conference on computational techniques, electronics and mechanical systems (CTEMS)* (IEEE, 2018), pp. 92–99



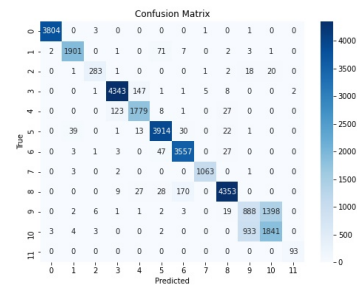
(a) MobileNet



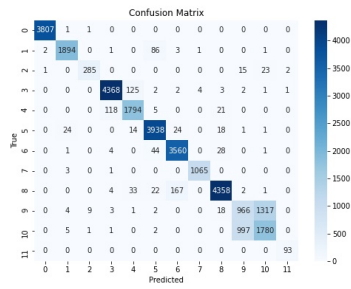
(b) MobileNetV2



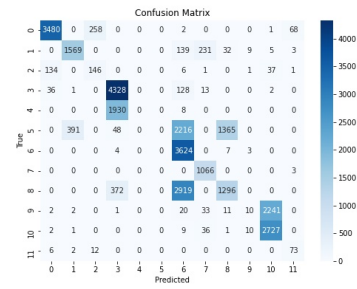
(c) MobileNetV3



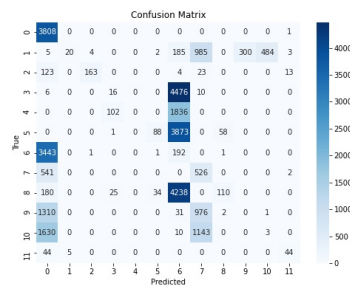
(d) DenseNet121



(e) DenseNet169



(f) EfficientNet-B0



(g) EfficientNet-B1

Fig. 9: Confusion matrices for all evaluated pre-trained architectures on multi-class DDoS detection.